AIP Journal of Applied Physics

Interface mechanics of adhesiveless microtransfer printing processes

H.-J. Kim-Lee, A. Carlson, D. S. Grierson, J. A. Rogers, and K. T. Turner

Citation: Journal of Applied Physics **115**, 143513 (2014); doi: 10.1063/1.4870873
View online: http://dx.doi.org/10.1063/1.4870873
View Table of Contents: http://scitation.aip.org/content/aip/journal/jap/115/14?ver=pdfcov
Published by the AIP Publishing

JOURNAL OF APPLIED PHYSICS **115**, 143513 (2014)

Interface mechanics of adhesiveless microtransfer printing processes

H.-J. Kim-Lee,[1,a)] A. Carlson,[2] D. S. Grierson,[1,b)] J. A. Rogers,[2] and K. T. Turner[1,3,c)]
[1]*Department of Mechanical Engineering, University of Wisconsin-Madison, Madison, Wisconsin 53706, USA*
[2]*Department of Materials Science and Engineering, Beckman Institute, and Frederick Seitz Materials Research Laboratory, University of Illinois at Urbana-Champaign, Urbana, Illinois 61801, USA*
[3]*Department of Mechanical Engineering and Applied Mechanics, University of Pennsylvania, Philadelphia, Pennsylvania 19104, USA*

(Received 3 February 2014; accepted 28 March 2014; published online 11 April 2014)

Microtransfer printing is a versatile process for retrieving, transferring, and placing nanomembranes of various materials on a diverse set of substrates. The process relies on the ability to preferentially propagate a crack along specific interfaces at different stages in the process. Here, we report a mechanics-based model that examines the factors that determine which interface a crack will propagate along in microtransfer printing with a soft elastomer stamp. The model is described and validated through comparison to experimental measurements. The effects of various factors, including interface toughness, stamp geometry, flaw sizes at the interfaces, and nanomembrane thickness, on the effectiveness of transfer printing are investigated using a fracture-mechanics framework and finite element modeling. The modeling results agree with experimental measurements in which the effects of interface toughness and nanomembranes thickness on the transfer printing yield were examined. The models presented can be used to guide the design of transfer printing processes. © *2014 AIP Publishing LLC*. [http://dx.doi.org/10.1063/1.4870873]

I. INTRODUCTION

Microtransfer printing is a versatile manufacturing technique that uses a stamp to retrieve patterned microstructures (i.e., nanomembranes) from a donor substrate and subsequently print the microstructures onto a receiver substrate (Fig. 1). Microtransfer printing enables the fabrication of high-performance flexible electronics, advanced packaging schemes, and complex 3D microstructures that cannot be realized with traditional fabrication techniques.[1–4] For transfer printing to be successful, the adhesion between the stamp and the nanomembrane (NM) must be controlled relative to the adhesion between the NM and the substrate. In the retrieval process, the stamp-NM interface must be strong relative to the NM-substrate interface, while for printing, the opposite must be the case.

High-yield transfer printing of solid objects can be achieved through the use of an adhesive to strongly bond the printed objects to the receiver substrate;[3] however, transfer printing without any adhesives has been demonstrated by exploiting the rate-dependent adhesion of a soft, viscoelastic stamp (e.g., polydimethylsiloxane (PDMS)).[5] Specifically, in the adhesiveless printing process, the adhesion between the stamp and the NM is controlled by the peeling rate of the stamp—high-speed peeling results in strong stamp-NM adhesion and is used for retrieval, while low-speed peeling leads to weak stamp-NM adhesion and is used for printing. While this adhesiveless process has many desirable attributes and has been used to fabricate a wide range of devices,[5–7] achieving high printing yield can be challenging in cases in which the adhesion between the NM and substrate is not sufficiently strong.[5,6] Numerous strategies for improving printing yield, including the application of shear during printing,[8,9] the use of stamps with reduced contact area,[6] and the use of complex structured stamps[2,7] have been reported. While these efforts have demonstrated routes to improve printing yield, there are undoubtedly other routes to increase the effectiveness of the printing process.[10] In order to understand the results reported to date and to uncover new strategies for improving the process, there is a critical need to establish a fundamental understanding of the mechanics of adhesiveless microtransfer printing.

The objective of this work is to establish the mechanics of soft-stamp microtransfer printing processes through an analysis of the factors that affect crack path selection in the process. While various aspects of the mechanics of the process have been previously discussed,[2,9,11] the problem of crack path selection in soft-stamp microtransfer printing has not been fully investigated. A nice framework for addressing the mechanics of transfer printing over a wide range of conditions is presented in Ref. 11, but that work did not provide a detailed analysis of the mechanics of soft stamp processes, in which the stamp and substrate modulus differ by a factor of approximately 10^4 to 10^5. In the present work, the mechanics of microtransfer printing processes utilizing a low-modulus ($E \sim 1$–4 MPa) elastomer stamp is analyzed with a fracture-mechanics approach using finite element (FE) modeling. The trends predicted by the model are compared to experimental results.

Throughout the paper, the experimental and modeled stamp and NM materials are PDMS and silicon, respectively. PDMS is the predominant material used in microtransfer printing processes and typically has a Young's modulus between 1 and 4 MPa. Silicon is chosen as the representative

[a)]Current address: Samsung Advanced Institute of Technology, Samsung Electronics, Yongin, Kyunggi-do, 446-712, South Korea.
[b)]Current address: SysteMECH, LLC, Madison, Wisconsin, 53705, USA.
[c)]Electronic mail: kturner@seas.upenn.edu

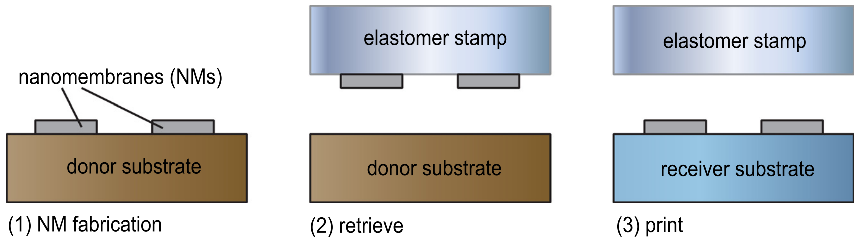

FIG. 1. Overview of the microtransfer printing process. (1) Microstructures/nanomembranes are fabricated and released on a donor substrate. (2) Retrieval process: an elastomer stamp is used to pick up the nanomembrane. For retrieval to be successful, crack propagation at the NM-substrate interface is required. (3) Printing process: the nanomembranes are placed onto the receiver substrate and separated from the stamp. For printing to be successful, crack propagation at the stamp-NM interface is required.

NM material here because silicon components are frequently transferred, and, with a Young's modulus of approximately 150 GPa, it has similar elastic properties to many inorganic nanomembranes. A general framework for examining the process mechanics is first established, and then the effects of the interface crack length, stamp geometry, interface toughness, and NM thickness on the success or failure of the printing process are investigated.

II. MECHANICS FRAMEWORK AND MODEL

A typical adhesiveless microtransfer process can be modeled as a system composed of three layers (a stamp, a nanomembrane, and a substrate) with two interfaces (stamp-NM, NM-substrate) as shown in Fig. 2. The system may be subjected to normal and shear loading during the retrieval and printing processes. The interfaces are substantially weaker than the bulk materials, thus cracks are assumed to propagate only along the interfaces. Success or failure in retrieval and printing is determined by the crack path selection between the two interfaces. In order for retrieval to be successful, it must be favorable for the crack to propagate along the lower interface in Fig. 2 (i.e., NM-substrate interface), while for printing to be successful, the system must be configured to cause the crack to propagate along the upper interface in Fig. 2 (i.e., stamp-NM interface).

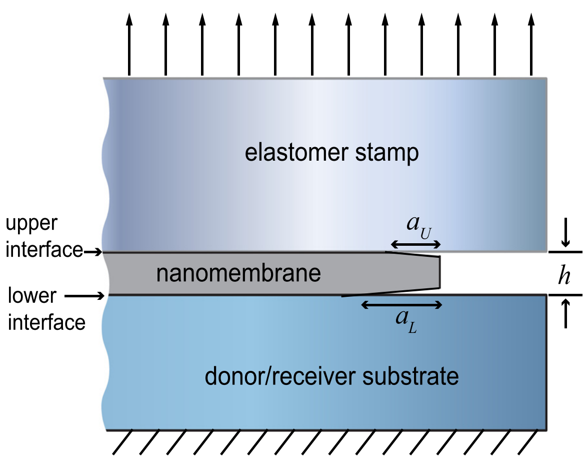

FIG. 2. Schematic of a basic transfer printing system illustrating the critical interfaces and components. There are three layers (stamp, nanomembrane, and substrate) and two interfaces. Retrieval and printing of the membrane is governed by the interface (upper or lower) along which the crack propagates when a load is applied to the system. The thickness of the printed layer is denoted as h, and the crack length at the upper and lower interfaces are denoted as a_U and a_L, respectively.

Based on fracture mechanics, the criterion for crack propagation along the upper and lower interfaces can be expressed in terms of a Griffith fracture criteria as $G_U \geq \Gamma_U$ and $G_L \geq \Gamma_L$, respectively, where G is the strain energy release rate, Γ is the interface toughness, and the subscripts U and L denote the upper and lower interfaces, respectively.[12] The strain energy release rate is a function of the geometry, loading, and elastic properties of the system, while the interface toughness describes the adhesion of the interface.

In a microtransfer printing process, the crack will propagate along the interface that reaches the failure criterion first as the load is applied to both interfaces in the system. The system that is considered here is assumed to be linear, thus the strain energy release rates at both interfaces scale with square of the applied load. As the applied load on the system is increased, the strain energy release rates on both interfaces will increase, and the interface with the larger G/Γ ratio will fail first. Thus, the conditions for printing and retrieval can be expressed as

$$G_U/G_L < \Gamma_U/\Gamma_L \quad \text{for retrieval (crack propagates at the lower interface)}, \tag{1}$$

and

$$G_U/G_L > \Gamma_U/\Gamma_L \quad \text{for printing (crack propagates at the upper interface)}. \tag{2}$$

A previous report used a similar criterion to develop a quality map for transfer printing for processes with a stiff silicon stamp and relatively long interface cracks.[11] This framework is used here to examine soft elastomeric stamps and relatively short interface cracks.

The above approach uses a simple Griffith energy balance to assess fracture at interfaces and neglects factors such as mixed-mode loading, which can be important in interface fracture problems. In general, the fracture resistance of an interface can depend on the relative amount of mode I (normal opening) and mode II (in-plane shear) loading at the interface. This dependence on mode mixity is typically described by considering the interface toughness to be a function of the phase angle of loading, $\Psi = \arctan(K_{II}/K_I)$, where K_I and K_{II} are the mode I and mode II stress intensity factors ($G = (K_I^2 + K_{II}^2)/E^*$, where E^* is the plane stress or plane strain modulus).[13,14] We calculated phase angles in this work, but do not consider them in the results presented as (1) all calculated phase angles were smaller than 25° for the cases studied and, within this range, the dependence of interface toughness on phase angle is weak for many material systems,[14] and (2) data for the phase angle dependence of PDMS-silicon interfaces have not been reported. If the interfaces were not substantially weaker than the other materials in the system, mode-mixity would play a larger role as the crack could potentially deviate from the interface into the stamp, membrane, or substrate. Another factor to be considered for crack propagation along bi-material interfaces is the second Dundur's parameter, which is a measure of the mismatch of the in-plane bulk modulus at a bi-material interface. This mismatch can affect the stress fields at the crack tip.[13,15] The bi-material interface in the microtransfer process is Si-PDMS, and the second Dundur's parameter in this case is close to zero (when $\nu_{stamp} = 0.49$). Therefore, the simple Griffith fracture criteria, $G_U \geq \Gamma_U$ and $G_L \geq \Gamma_L$, are used throughout this work.

G_U and G_L values are calculated using FE modeling and the virtual crack closure technique (VCCT)[16] with the mesh structures shown in Figs. 3(a) and 3(b). The VCCT is a widely used method to compute energy release rates from 2D and 3D finite element analyses. It uses the length of the element near the crack tip, the reaction forces at the nodes in front of the crack tip, and the displacements at the nodes behind the crack tip calculated from FE modeling to obtain G values. Detailed application of this technique depends on the type of elements and models that are used. In this work, the formulation and equations reported by Krueger[16] were used.

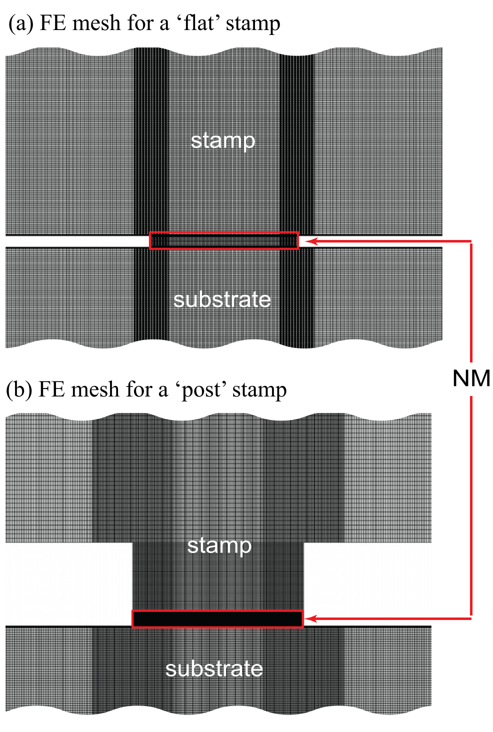

FIG. 3. Mesh geometries used in the finite element analysis. Two different stamp geometries are studied: (a) 'Flat' and (b) 'post.'

Two different stamp geometries, 'flat' and 'post,' which correspond to common experimental geometries, are examined. The 'flat' stamps do not have any pattern on the stamp surface, while 'post' stamps have posts with a height of 50 μm and lateral dimensions that match the microstructures being printed. The thickness of the stamp, the thickness of the substrate, and the width of the NM layer are fixed at 1 mm (including post height in the post stamp), 500 μm, and 100 μm, respectively. The thickness of the NM (h in Fig. 2) is varied from 0.1–10 μm. The model is composed of 2D plane strain, eight-node, quadratic, rectangular elements and has periodic boundary conditions on the left and right side of the model. The model was developed and solved using the commercial FE package ABAQUS^{TM}. The materials are assumed to be isotropic, linear elastic and are defined in terms of Young's modulus, E, and Poisson's ratio, ν. The materials for the stamp and NM are PDMS and Si. The Young's modulus and Poisson's ratio used for the stamp layer are $E_{stamp} = 2.1$ MPa and $\nu_{stamp} = 0.49$, while those of the NM are $E_{NM} = 148$ GPa and $\nu_{NM} = 0.18$ (average in-plane elastic properties of a (100) Si membrane). For the substrate, the mechanical properties used are those of either Si (same E and ν as those of the NM) or glass, with $E_{glass} = 70$ GPa and $\nu_{glass} = 0.3$.

Loading was applied in the normal direction by prescribing displacements at the top of the stamp while holding the bottom of the substrate fixed (Fig. 2). The interfaces were modeled as perfectly bonded, i.e., the displacements were coupled between the two materials at the interface. An initial crack was included at the edge of the interface by removing the coupling constraint between the layers over the length of the initial crack. Reaction forces and displacements were calculated along the interfaces. The VCCT, as described above, was subsequently used to calculate G_U and G_L from the FE results for forces and displacements near the crack tips.[16] The initial cracks, introduced at both sides of the NM, were varied in length from 0.01–10 μm at both interfaces (a_U and a_L denote the precrack lengths at the upper and lower interfaces, respectively). The mesh was selected through a convergence study in which the FE models were solved with a mesh that was refined by a factor of 10 for the models with precracks from 0.1–10 μm. The finer mesh resulted in less than a 2% difference in calculated G values, thus the mesh was considered sufficient. For the model with a precrack of 0.01 μm, the mesh density was only doubled in the convergence study, due to computational limitations. Doubling the mesh density resulted in less than a 0.1% change in G values, again suggesting the mesh was adequate. In any single simulation, strain energy release rates were calculated with the assumption that the crack exists only at one interface. G_U/G_L is calculated for different combinations of upper and lower precrack lengths and compared to the ratio of the toughness values of the upper and lower interfaces, Γ_U/Γ_L.

III. RESULTS AND DISCUSSION

A. Effect of crack length and nanomembrane geometry

Strain energy release rates at the upper and lower interfaces for different precrack lengths were calculated under pure normal loading for a system consisting of a flat slab of PDMS as the stamp, a thin Si layer as the NM, and glass as the substrate. Since the stamp and substrate are at least 50-times thicker than the NM layer in this study, G_U and G_L are expected to depend primarily on the crack length (a_U or a_L) and the NM geometry (thickness, h, and width, w). Normalized G_U and G_L are plotted as a function of a_U/h and a_L/h in Figs. 4(a) and 4(b), respectively. While both plots show that the strain energy release rates increase with the crack length, G_U and G_L exhibit a different dependence on the ratio of the crack length to NM thickness. Fig. 4(b) shows that the same a_L/h values result in almost the same G_L, however, G_U values in Fig. 4(a) vary significantly with membrane thickness, h, for the same a_U/h. The strain energy release rate at the upper interface, G_U, appears to be determined by a_U alone as shown in Fig. 4(c). In general, G_U is influenced by both a_U and w, however the effect of varying w is not examined in the present study.

The dependence of G_U on crack length can be calculated analytically from established solutions for "cracks at the joint of a strip and semi-infinite plate" that approximates the geometry of the transfer-printing elements.[17,18] The configuration shown in Fig. 2 can be approximated as a stiff strip of width w bonded to an extremely compliant semi-infinite plate with a crack of length a_U at the interface between the stiff strip and compliant substrate. Using the solutions in Refs. 17 and 18, the mode I and II stress intensity factors (K_I and K_{II}) can be calculated for a given crack length, a_U, and NM width, w. The strain energy release rate, G_U, is then obtained as

$$G_U = \frac{1}{2E_{stamp}}\left({K_I}^2 + {K_{II}}^2\right). \quad (3)$$

The above calculation of the strain energy release rate from the stress intensity factors includes a factor of 1/2 due to the fact that the crack is at a bimaterial interface in which the elastic modulus of one layer (the stamp) is several orders of magnitude smaller than that of the other layer (NM-substrate pair).[19,20] The results of the analytical calculation (Fig. 4(d)) have a similar trend and magnitude to the FE results (Fig. 4(c)). The differences that are present are not surprising given that the geometries considered in the analytical and finite element models are slightly different. In both the analytical and FE results, G_U decreases rapidly as a_U decreases, however, there is little change in G_U for a_U less than 1 μm. The insensitivity of G_U to crack length at small crack lengths mitigates the effect of uncertainty in initial crack length at the upper interface when comparing experiment and model results. While it is difficult to measure the crack length at the interface in experiments, the crack is expected to be very small at the upper interfaces because the extremely compliant elatsomer stamp can conform to imperfections on the surfaces of the membrane. Given the insensitivity of G_U to crack length for a_U less than 1 μm and the ability of PDMS to conform to surface defects, we use $a_U = 0.01$ μm in all subsequent strain energy release rate calculations in this paper.

The ratio of the strain energy release rates at the upper and lower interfaces, G_U/G_L, rather than individual values of G_U or G_L, must be examined to assess crack path selection and transfer printing yield. In Figs. 5(a) and 5(b), G_U/G_L is shown as a function of a_L/h for a flat stamp and a post stamp, respectively. G_L values increase with increasing a_L/h while G_U does not significantly change, thus G_U/G_L decreases as a_L/h increases for both stamp geometries. The post and flat stamp cases both exhibit similar trends with a_L/h, however, the strain energy release rate ratios are, overall, lower for post-type stamps. This suggests that post stamps would offer advantages for retrieval of NMs, while flat stamps would be better for printing.

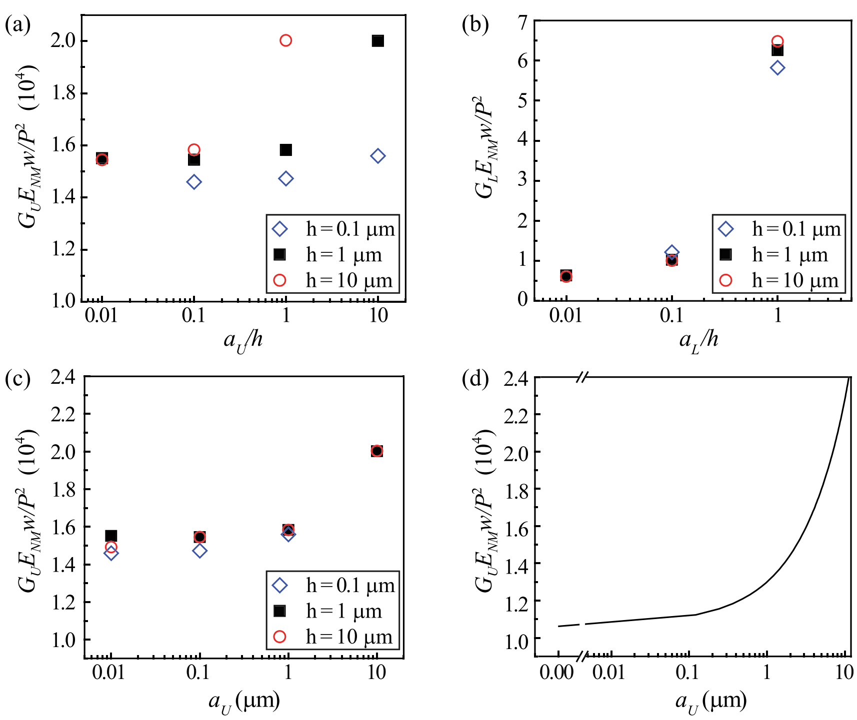

FIG. 4. Strain energy release rates at the upper and lower interfaces as a function of crack length. (a) G_U vs. a_U/h for h from 0.1 to 10 μm. (b) G_L vs. a_L/h for h from 0.1 to 10 μm. (c) G_U vs. a_U. Note that G_U does not change significantly with a_U when a_U is sufficiently small (<1 μm). (d) Results from a simplified analytical model, showing normalized G_u vs. a_U. A similar trend with the results of (c) is observed. In all plots, the strain energy release rate is normalized in terms of the width of the nanomembrane, w, the modulus of the nanomembrane, E_{NM}, and the applied normal load per unit depth, P.

B. Effect of interface toughness

To examine the validity of the model presented above, we first compare our predictions to previously reported experimental measurements in which the effective interface toughness between the stamp and NM was varied through patterning of the stamp. Transfer printing yields for stamps with different contact area fractions (AF) were measured by Kim *et al.*,[6] and the results from this previous work are summarized in Fig. 6(a). The printing yield of 300-nm-thick Si ribbons was measured to be about 20% when the stamp had 100% contact area fraction (i.e., a flat, unpatterned stamp) and yield increased to 92% as the contact area was reduced by placing narrow, shallow reliefs on the surface of the stamp to reduce the contact area fraction to 40% (Fig. 6(a)). A reduction in the contact area between the stamp and NM effectively results in a reduction of toughness of the upper interface, Γ_U. Within the fracture-mechanics framework presented above, printing is expected to occur when $G_U/G_L > \Gamma_U/\Gamma_L$. In experiments, there will be a statistical distribution in each of the quantities in the printing criterion due to variations in fabrication, surface cleanliness, roughness, etc. Thus, we expect that higher printing yield will be achieved as G_U/G_L is increased relative to Γ_U/Γ_L.

Strain energy release rate ratios, G_U/G_L, were calculated using the FE model described in Sec. II, for the experimental configuration detailed in Ref. 6: A PDMS stamp, a 300-nm-thick Si membrane, a Si substrate as a donor, and a glass slide as a receiver substrate. The crack length at the lower interface (a_L) was varied from 0.01 to 2 μm in the simulations because the exact value is not known; a_U is fixed at 0.01 μm as discussed Sec. III A. The calculated G_U/G_L values are shown as black squares in Fig. 6(b). In order to assess if printing or retrieval will occur, values for Γ_U and Γ_L are also needed. The lower interface during the retrieval step is between two hydrogen-terminated silicon surfaces (resulting from the release of the membranes using hydrofluoric acid); an approximate interface toughness for such an interface is 5 mJ/m^2.[21] During the printing step, the lower interface is between a smooth silicon surface and a relatively rough glass microscope slide; the interface toughness for this case is estimated to be approximately 1 mJ/m^2.[22] The upper interface in both the retrieval and printing steps is between PDMS and silicon. The PDMS-Si interface toughness is rate-dependent and can vary from $\sim$100 mJ/m^2 with a slow crack propagation rate ($\sim$1 mm/s in 90° peel test) used for printing, to $\sim$15 000 mJ/m^2 with a fast crack propagation rate ($\sim$25 cm/s in 90° peel test) used for retrieval.[6] Thus, Γ_U/Γ_L for retrieval and printing is estimated to be $\sim$3000 and $\sim$100, respectively. The two dashed lines in Fig. 6(b) represent these Γ_U/Γ_L ratios and provide the upper limit for retrieval and the lower limit for printing when the contact area fraction of the stamp is 100%. At 100% area fraction, conditions would be ideal for transfer printing if $a_L = 1$ μm as the corresponding G_U/G_L ratio for this a_L is between the retrieval and printing bounds (Fig. 6(b)). If the contact area fraction of the stamp is 40%, the effective toughness at the upper interface, Γ_U decreases by 60% and the

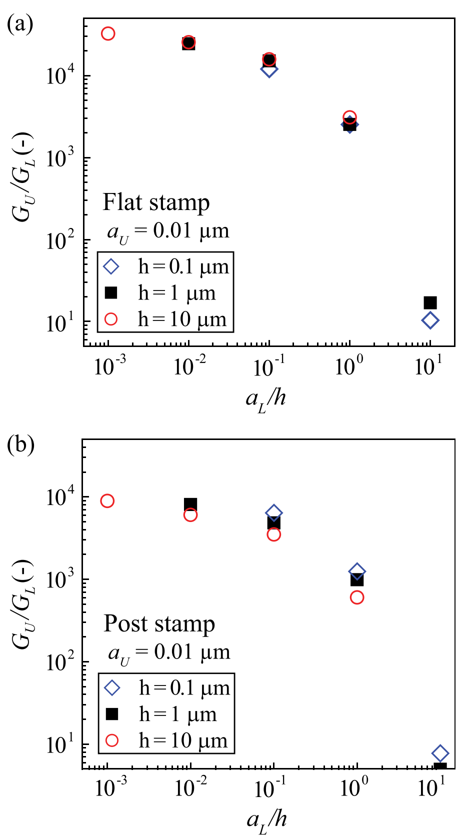

FIG. 5. (a) G_U/G_L vs. a_L/h for a flat stamp geometry. G_U/G_L decreases as a_L increases because G_L increases significantly with large a_L. Results are shown for $E_{stamp} = 2.1$ MPa, $\nu_{stamp} = 0.49$, $E_{sub} = 148$ GPa, and $\nu_{sub} = 0.18$. (b) G_U/G_L vs. a_L/h for the post stamp geometry. Results for the post stamp generally exhibit a trend that is similar to the results of the flat stamp.

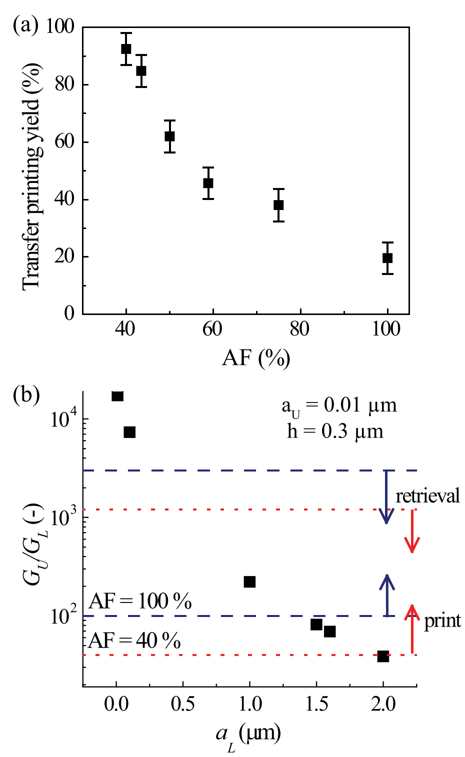

FIG. 6. (a) Transfer printing yield for different contact area fractions (AF) of the flat stamp reported in the work of Kim *et al.*[6] (b) G_U/G_L as a function of the crack length at the lower interface, a_L, calculated by FE modeling. The crack lengths of $a_L = 1.5$–1.9 μm provides agreement with the experimental results, and this crack length range is physically reasonable.

retrieval and printing bounds shift. The upper and lower limits for successful transfer printing with a stamp that has a contact area fraction of 40% are shown as the two dotted lines in Fig. 6(b).

The measured transfer printing yields (Fig. 6(a)) can be compared with the calculated G_U/G_L and Γ_U/Γ_L ratios (Fig. 6(b)) in order to gain insight into the mechanics of the printing process and to estimate the effective crack length at the lower interface for this particular experimental system. In the reported experiment, the retrieval process did not pose a challenge,[6] so the analysis here is focused on printing. Assuming that the G_U/G_L and Γ_U/Γ_L ratios have the same type of probability distribution function, when the mean value of G_U/G_L is equal to the mean value of Γ_U/Γ_L, the printing yield will be 50%. The printing yield will be higher than 50% if $G_U/G_L > \Gamma_U/\Gamma_L$, and lower than 50% if $G_U/G_L < \Gamma_U/\Gamma_L$. The experimental results in Fig. 6(a) show that printing yield increases as the stamp-membrane contact area, and correspondingly the effective Γ_U/Γ_L, decreases. The crack length at the lower interface can be estimated by recognizing that the printing yield is far less than 50% when the contact area fraction is 100%, and the yield is well above 50% when the area fraction is 40%. This suggests that the G_U/G_L ratio of the system must be between the printing limits of the 40% stamp (lower dotted line in Figure 6(b)) and the 100% stamp (lower dashed line in 6(b)). Based on the FE calculations shown in Fig. 6(b), the range of crack lengths that would result in a G_U/G_L between these limits is $a_L = 1.5$–$1.9\,\mu$m. Given that the Si NM is being printed onto a rougher glass surface in these experiments, it is reasonable for a_L to be in the micrometer range. It is also important to realize that the mechanics model presented here is a 2D analysis and does not capture the full complexity of edge flaws in the real 3D system. Thus, the precrack length, a_L, in the 2D model should be viewed as an effective defect size at the lower interface and can be determined from comparison to experimental data, as shown in Fig. 6.

C. Effect of nanomembrane thickness

The thickness of the NM can affect transfer printing process performance. Here, the effect of NM thickness on printing performance is examined using both FE simulations and transfer printing experiments. Beyond being an important parameter in transfer printing processes, the effect of NM thickness is investigated here because it is a variable that can be controlled independently in experiments and thus is well-suited for making quantitative comparisons between the model and experiments. Most other parameters in the micro-transfer printing process change multiple aspects of the process and therefore cannot be investigated independently in experiments (for example, changing the Young's modulus by altering the material of the stamp can also affect Γ_U and a_U).

In the experiments, $100\,\mu m \times 100\,\mu m$ Si NMs with thicknesses of $h = 70$, 320, 700, 1250, and 3000 nm were transfer printed onto both glass and Si substrates. The yield during the printing step was quantified as a function of NM thickness. Specimen preparation and transfer printing were performed using the process described in Carlson *et al.*[8] The post stamps were sized to the NMs and had lateral dimensions of $100\,\mu m \times 100\,\mu m$ and a height of $50\,\mu$m. During printing, a shear load was applied along with the normal load on the stamp to facilitate release of the membrane as described in Ref. 8.

FE calculations are performed for the same stamp geometries and loading conditions as the experiments using the model described in Sec. II. The models are 2D, and the precrack lengths at the upper and lower interfaces are assumed to be $0.01\,\mu$m and $1.5\,\mu$m, respectively. A shear displacement of $12.5\,\mu$m is combined with a normal displacement of approximately $7\,\mu$m, leading to $G_U = 100\,\mathrm{mJ/m^2}$, which is expected to cause delamination at upper interface at low peel speeds. Two different values were used for the lower interface toughness: $\Gamma_L = 1\,\mathrm{mJ/m^2}$ for the glass substrate and $\Gamma_L = 100\,\mathrm{mJ/m^2}$ for the Si substrate. The glass substrate has a lower effective toughness because the surface is rougher than that of the Si substrate. The results of the modeling are shown in Fig. 7(a) in terms of the ratio of (G_U/G_L) to (Γ_U/Γ_L) as a function of the thickness of the NM layer. As

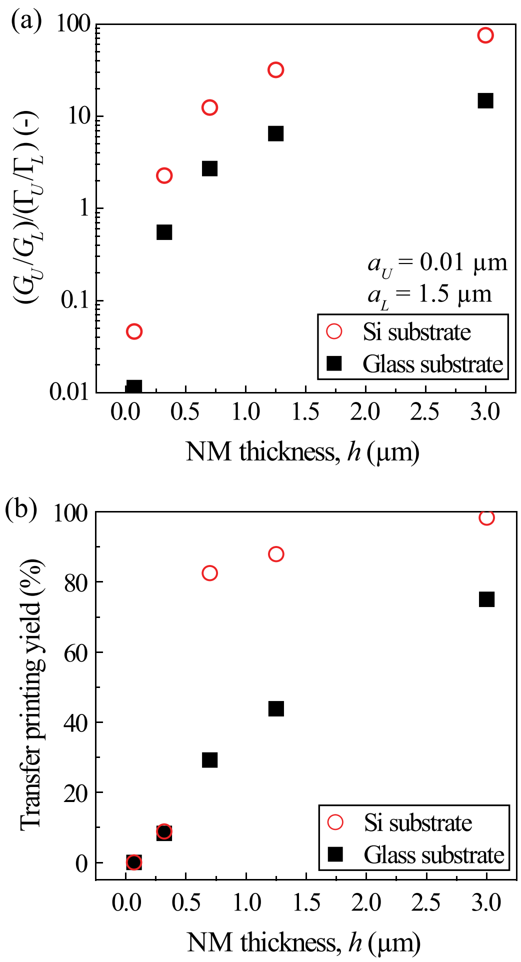

FIG. 7. (a) FE calculation of $(G_U/G_L)/(\Gamma_U/\Gamma_L)$ as a function of nanomembrane thickness. (b) Experimentally measured printing yield for Si membranes on Si and glass substrates. The yields were calculated from 58 and 48 tests per condition for printing on Si and glass substrate, respectively. Both the modeling results and the experimental measurements show that the yield increases with increasing NM thickness. Note, that thin membranes (<100 nm) are often transferred using more complex stamp geometries or sacrificial layers that increase the effective thickness.

the condition for printing (failure at the lower interface) is $G_U/G_L > \Gamma_U/\Gamma_L$, the ratio of (G_U/G_L) to (Γ_U/Γ_L) serves as a measure of printability. Therefore, Figure 7(a) suggests that the printing yield should increase with increasing NM thickness.

The experimental results (Fig, 7(b)) exhibit a similar trend to the modeling results and show an increase in printing yield with increasing NM thickness. The experimental results also show that printing yield is generally higher and changes more dramatically with NM thickness when printing on a Si substrate compared to the glass substrate. The overall higher yield can be understood from the modeling results in Fig. 7(a) which shows that the ratio of (G_U/G_L) to (Γ_U/Γ_L) for printing on a Si substrate is larger than that for printing on a glass substrate. This is primarily due to the higher roughness of the glass substrate, which reduces the effective toughness of the NM-substrate interface. Also, the measured yield on the Si substrate tests increases sharply between NM thicknesses of 320 nm and 700 nm, while the measured yield increases more gradually with increasing NM thickness on the glass substrate. We believe that the transition is sharper on the silicon substrate, which is a semiconductor grade silicon wafer, because the substrate has lower and more uniform roughness than the glass substrate, which is a standard microscope slide. As such, there is less statistical variation in the toughness of NM-substrate interface in the silicon substrate tests and the transition from non-printing to printing is sharper. The overall agreement between the experimental and modeling results suggests that the modeling framework and FE models described in Sec. II can be used to predict the effect of NM geometry on transfer printing process performance.

The experiments here show that transfer printing of Si membranes that are thinner than 100 nm is difficult with the stamp and loading configuration used here. However, it is important to note that there are many demonstrations of the transfer of thin NM layers (<100 nm). Transfer of thin layers can be achieved using sacrificial layers (e.g., photoresist) that increase the thickness of the part being transferred and through the use of advanced stamp geometries and printing processes.

IV. CONCLUSIONS

This work has used a fracture mechanics framework to investigate factors that affect retrieval and printing of NMs with soft stamps in microtransfer printing processes. This framework shows that while it is important to control the interface adhesion in the processes to achieve high-yield retrieval and printing, the geometry of the NM layer, as well as the geometries of the stamp and substrate, also affect which interface the crack propagates at and are critical in transfer printing process design. The ratio of strain energy release rates, G_U/G_L, and the ratio of interface toughness values, Γ_U/Γ_L, at the upper and lower interfaces are the critical factors that determine transfer printing performance. The analyses presented illustrate the effect of several important parameters: (1) The initial crack length (relative to the NM layer thickness) at the NM-substrate interface strongly affects the strain energy release rates, while the initial crack length at the stamp-NM interface does not if it is sufficiently small ($a_U < \sim 1\ \mu$m for the geometries examined here); (2) a lower interface toughness at the stamp-NM interface is desirable for printing; and (3) increasing the thickness of the NM layer increases the strain energy release rate at the upper interface relative to the lower interface and therefore increases printing yield. The second and third points have also been demonstrated with experimental measurements. The modeling analyses used here provide a route to map out the process conditions for successful transfer printing with soft elastomer stamps.

ACKNOWLEDGMENTS

We thank Professor Yonggang Huang of Northwestern University for helpful discussions. This work was supported by NSF CMMI #0845294 and AFOSR-MURI FA9550-08-1-0337 (A. Carlson acknowledges support from the Department of Defense through the National Defense Science and Engineering Graduate (NDSEG) Fellowship program.)

[1] K. J. Lee, M. J. Motala, M. A. Meitl, W. R. Childs, E. Menard, A. K. Shim, J. A. Rogers, and R. G. Nuzzo, Adv. Mater. **17**, 2332 (2005).
[2] S. Kim, J. Wu, A. Carlson, S. H. Jin, A. Kovalsky, P. Glass, Z. Liu, N. Ahmed, S. L. Elgan, W. Chen, P. M. Ferreira, M. Sitti, Y. Huang, and J. A. Rogers, Proc. Natl. Acad. Sci. U.S.A. **107**, 17095 (2010).
[3] A. J. Baca, J.-H. Ahn, Y. Sun, M. A. Meitl, E. Menard, H.-S. Kim, W. M. Choi, D.-H. Kim, Y. Huang, and J. A. Rogers, Angew. Chem. Int. Ed. Engl. **47**, 5524 (2008).
[4] J.-H. Ahn, H.-S. Kim, K. J. Lee, S. Jeon, S. J. Kang, Y. Sun, R. G. Nuzzo, and J. A. Rogers, Science **314**, 1754 (2006).
[5] M. A. Meitl, Z.-T. Zhu, V. Kumar, K. J. Lee, X. Feng, Y. Y. Huang, I. Adesida, R. G. Nuzzo, and J. A. Rogers, Nature Mater. **5**, 33 (2006).
[6] T.-H. Kim, A. Carlson, J.-H. Ahn, S. M. Won, S. Wang, Y. Huang, and J. A. Rogers, Appl. Phys. Lett. **94**, 113502 (2009).
[7] S. Kim, A. Carlson, H. Cheng, S. Lee, J.-K. Park, Y. Huang, and J. A. Rogers, Appl. Phys. Lett. **100**, 171909 (2012).
[8] A. Carlson, H.-J. Kim-Lee, J. Wu, P. Elvikis, H. Cheng, A. Kovalsky, S. Elgan, Q. Yu, P. M. Ferreira, Y. Huang, K. T. Turner, and J. A. Rogers, Appl. Phys. Lett. **98**, 264104 (2011).
[9] H. Cheng, J. Wu, Q. Yu, H.-J. Kim-Lee, A. Carlson, K. T. Turner, K.-C. Hwang, Y. Huang, and J. A. Rogers, Mech. Res. Commun. **43**, 46 (2012).
[10] R. Li, Y. Li, C. Lü, J. Song, R. Saeidpouraza, B. Fang, Y. Zhong, P. M. Ferreira, J. A. Rogers, and Y. Huang, Soft Matter **8**, 3122 (2012).
[11] M. B. Tucker, D. R. Hines, and T. Li, J. Appl. Phys. **106**, 103504 (2009).
[12] A. Griffith, Philos. Trans. R. Soc. London, A **221**, 163 (1921).
[13] J. W. Hutchinson and Z. Suo, Adv. Appl. Mech. **29**, 63 (1992).
[14] M. D. Thouless and Q. D. Yang, in *Mechanics of Adhesion*, edited by D. A. Dillard and A. V. Pocius, 1st ed. (Elsevier, New York, 2002), pp. 235–271.
[15] J. Dundurs, J. Appl. Mech. **36**, 650 (1969).
[16] R. Krueger, Appl. Mech. Rev. **57**, 109 (2004).
[17] N. Hasebe and M. Takemura, Eng. Fract. Mech. **15**, 45 (1981).
[18] H. Tada, P. Paris, and G. Irwin, *The Stress Analysis of Cracks Handbook*, 3rd ed. (ASME Press, New York, 2000).
[19] Y. Y. Huang, W. Zhou, K. Hsia, E. Menard, J.-U. Park, J. A. Rogers, and A. G. Alleyne, Langmuir **21**, 8058 (2005).
[20] J. R. Rice, J. Appl. Mech. **55**, 98 (1988).
[21] A. Plößl and G. Kräuter, Mater. Sci. Eng., R **25**, 1 (1999).
[22] T.-K. Chuang, A. Usenko, and J. S. Cites, ECS Trans. **33**, 501 (2010).